Supporting Information

Anisotropic X-ray Detection Performance of Melt-grown $CsPbBr_3$ Single Crystal

Yunqiu Hua,† Xue Sun,† Xiang Li, Fucai Cui, Zhongjie Yue, Jiaxin Liu, Hongjie Liu, Guodong Zhang, and Xutang Tao**

Y. Q. Hua, X. Sun, X. Li, F. C. Cui, Z. J. Yue, J. X. Liu, H. J. Liu

Prof. G. D. Zhang, Prof. X. T. Tao

State Key Laboratory of Crystal Materials

Institute of Crystal Materials

Shandong University

Jinan 250100, PR China

E-mail: zgd@sdu.edu.cn

txt@sdu.edu.cn

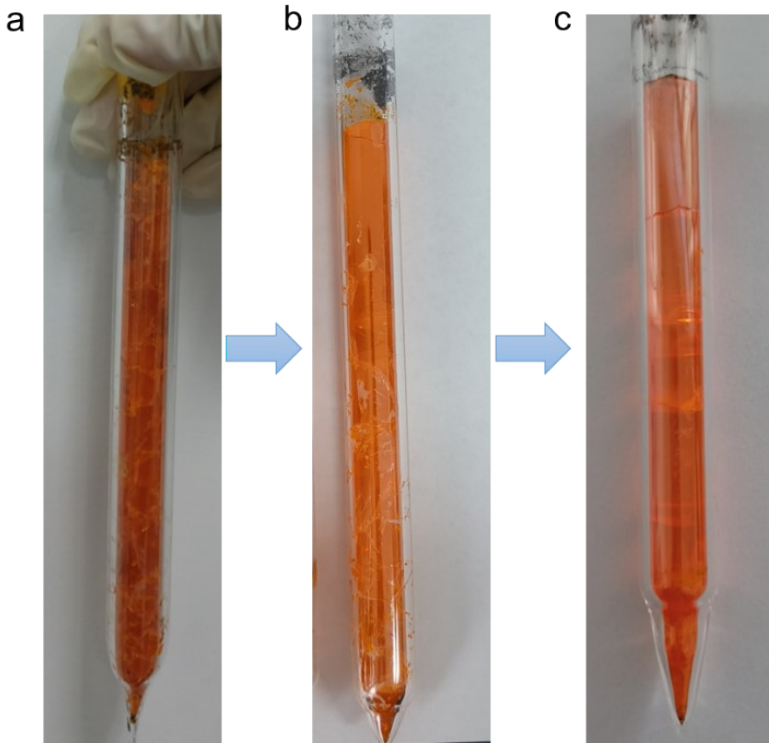

Fig. S1 $CsPbBr_3$ polycrystal purified for (a) the first time, (b) the second time, and (c) the third time.

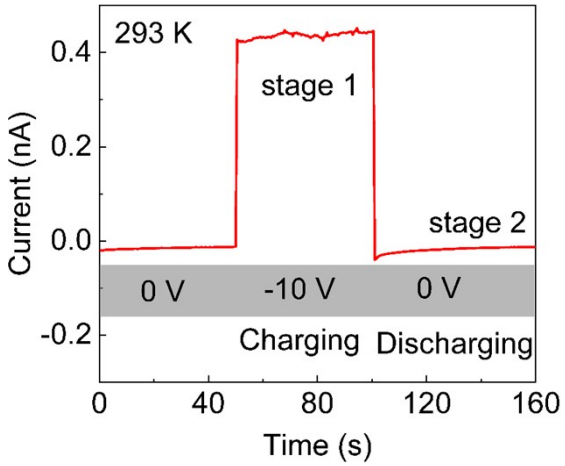

Fig. S2 Schematic and typical charging-discharging process curve of $CsPbBr_3$ single crystal.

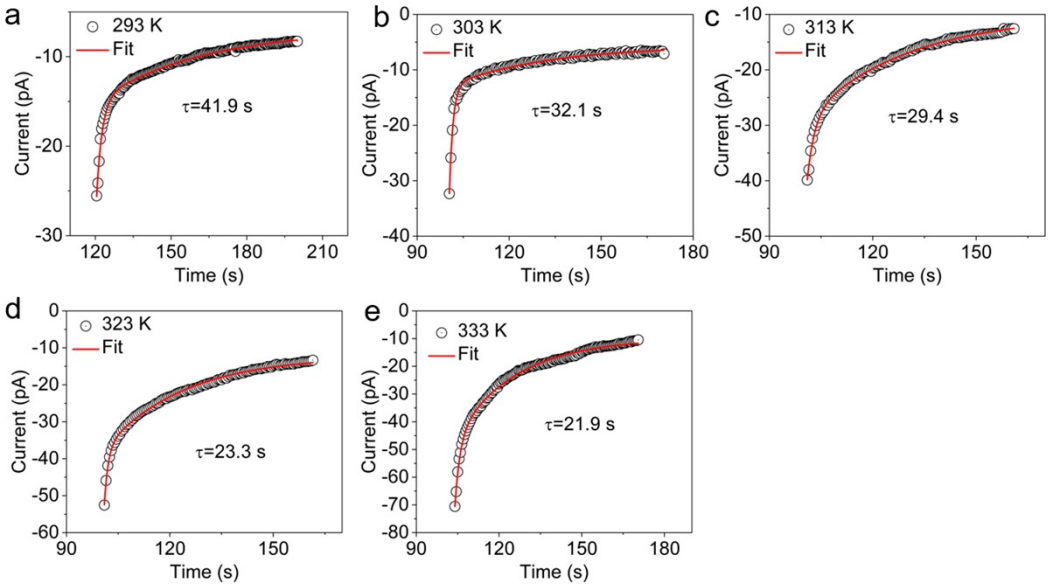

Fig. S3 The representative temporal response curves of stage 2 at various temperatures from 293 to 333 K for [100] orientation of $CsPbBr_3$ single crystal.

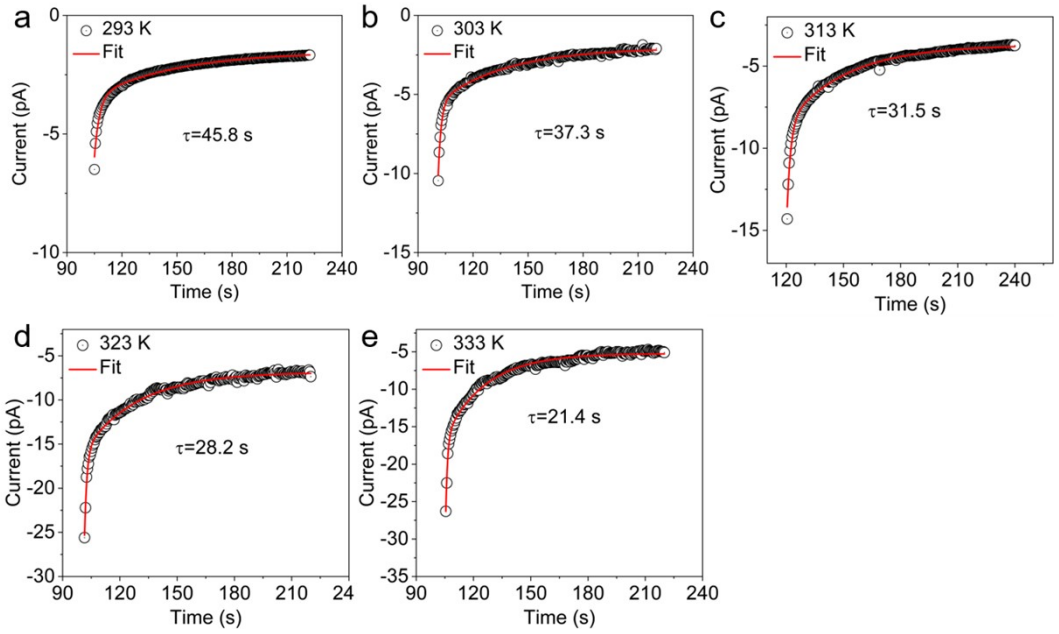

Fig. S4 The representative temporal response curves of stage 2 at various temperatures from 293 to 333 K for [010] orientation of $CsPbBr_3$ single crystal.

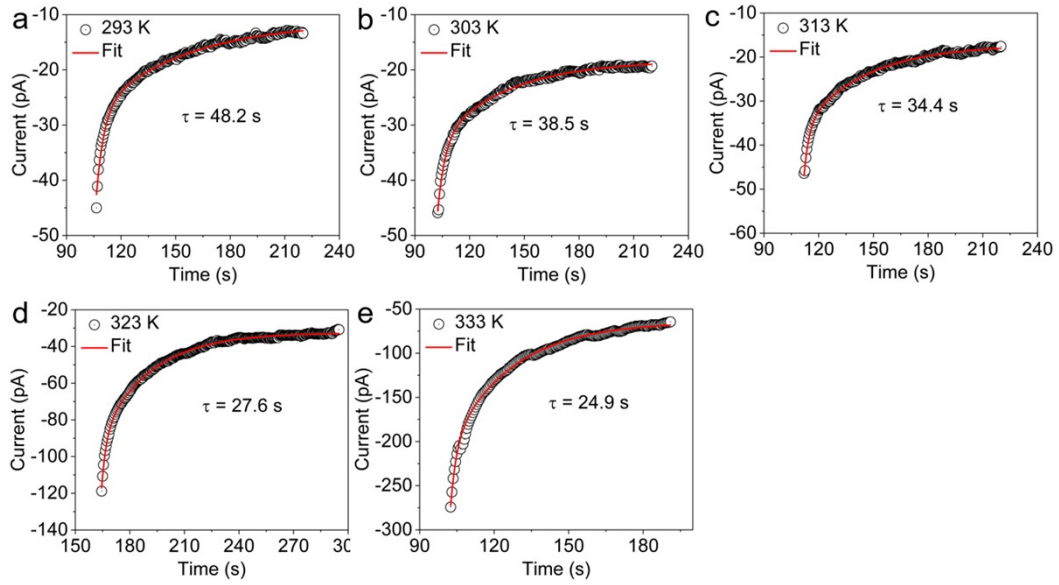

Fig. S5 The representative temporal response curves of stage 2 at various temperatures from 293 to 333 K for [001] orientation of $CsPbBr_3$ single crystal.

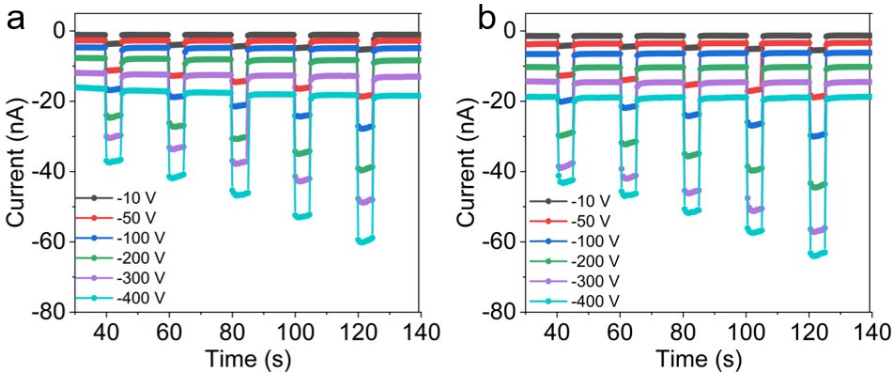

Fig. S6 Temporal X-ray responses under various voltages from -10 V to -400 V for the device based on the (a) (100) and (b) (001) wafers of the $CsPbBr_3$ single crystal.

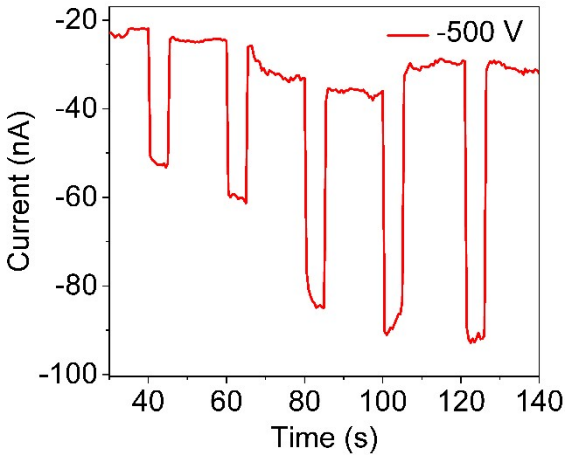

Fig. S7 Photocurrent-dose rate curves of the (010) detector under -500 V.

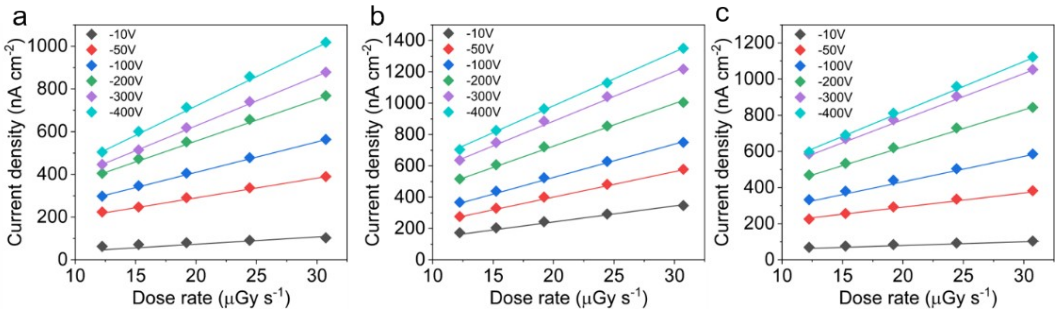

Fig. S8 Photocurrent response at different reverse biases under 120 keV X-ray various dose rates of the (a) (100), (b) (010), and (c) (001) detectors, respectively.

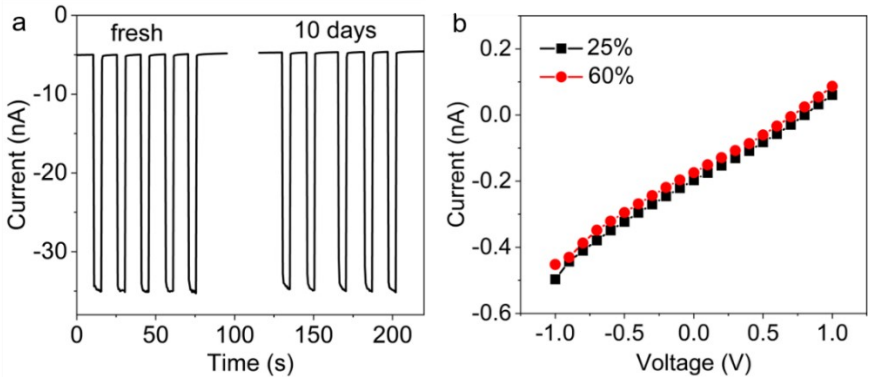

Fig. S9 (a) X-ray response stability of $CsPbBr_3$ detector under -100 V at room temperature. (b) *I-V* curves of $CsPbBr_3$ crystal device when the humidity is at 25% and 60%.